Bridging the gap from mononuclear Pd^{II} precatalysts to Pd nanoparticles: Identification of intermediate linear $[Pd_3(XPh_3)_4]^{2+}$ clusters as catalytic species for Suzuki-Miyaura couplings (X = P and As)

Kate M. Appleby,[†,‡] Evans Dzotsi,[‡] Neil W. J. Scott,[‡] Guan Dexin,[†] Neda Jeddi,[‡] Adrian C. Whitwood, [‡] Natalie E. Pridmore,[‡] Sam Hart,[‡] Simon B. Duckett[†,‡*] and Ian J. S. Fairlamb[‡*]

† Centre for Hyperpolarisation, University of York, York, North Yorkshire, YO10 5NY, United Kingdom

‡ Department of Chemistry, University of York, York, North Yorkshire, YO10 5DD, United Kingdom.

ABSTRACT: Tri-palladium clusters, of the type $[Pd_3(PPh_3)_4]^{2+}$, wherein three linearly-connected Pd atoms are stabilized by phosphine and arsine ligands, have been detected and isolated as intermediates during the reduction of well-defined mononuclear $[Pd(OTf)_2(XPh_3)_2]$ (X = P or As respectively) to Pd nanoparticles (PdNPs). The isolated $[Pd_3(PPh_3)_4]^{2+}$ cluster isomerizes on broadband UV irradiation to form an unexpected photoisomer, produced by a remarkable change in conformation at one of the bridging PPh_3 ligands. A catalytic role for these $[Pd_3(XPh_3)_4]^{2+}$ species is exemplified in Suzuki-Miyaura cross-coupling (SMCC) reactions, with high activity seen in the arylation of a brominated heterocyclic 2-pyrone. Use of the $[Pd_3(PPh_3)_4]^{2+}$ cluster enables a switch in site-selectivity for SMCC reactions involving 2,4-dibromopyridine from the typical C2-bromide site (seen previously for mononuclear Pd catalysts) to the atypical C4-bromide site thereby mirroring recently reported cyclic Pd_3 clusters and PdNPs. We have further determined that thermal and photoisomers of $[Pd_3(PPh_3)_4]^{2+}$ are similarly catalytically active in the Pd-catalyzed hydrogenation of phenylacetylene to give styrene. Our findings link the evolution of mononuclear Pd(II) salts to PdNPs via the intermediacy of linear $[Pd_3(XPh_3)_4]^{2+}$ clusters.

Introduction

Palladium (Pd) catalyzes an eclectic array of reactions, including hydrogenation, hydroformylation, cyanation and cross-coupling reactions, from traditional modification of C-X bonds with organometallic compounds to the functionalization of pluripotent C–H bonds.[1] With many research teams recently focusing on earth abundant metals, there is a strong impetus to better utilize precious Pd in catalytic applications (projected for continued use in industrial processes for at least another 20 to 30 years). In this context, understanding pre-catalyst activation, catalyst speciation changes and catalyst deactivation is critically important. For many catalytic cross-coupling reactions the true active catalysts have been debated intensely.[2] Early mechanistic hypotheses assumed a homogeneous behavior and a simple catalytic cycle, involving mononuclear Pd species, as the exclusive pathway. However, it is now widely accepted that the real situation is far more complicated than this early 'textbook' mechanistic hypothesis. For example, several experimental studies support a quasi-heterogeneous catalyst regime,[3] with some providing experimental evidence for heterogeneous behavior, *i.e.* agglomerated Pd species that allow surface catalysis are not simply a moribund form of Pd. Catalyst speciation changes are not just limited to general cross-coupling reactions. Indeed, experimental evidence has demonstrated that Pd nanoparticles (NPs)[4] are able to mediate C-H bond functionalization reactions, despite early mechanistic investigations focusing solely on catalytic cycles that operate with mononuclear Pd intermediates. Furthermore, Corma *et al.* have reported experimental evidence that small Pd clusters are active in a variety of cross-coupling reactions, whose formation from stabilized PdNPs is promoted by water.[5]

Most mechanistic arguments focus on these two extremes for cross-coupling processes, *i.e.* mononuclear Pd_1 species versus higher order PdNPs. Only a few studies have examined the potential role small Pd_n clusters ($n<5$) that bridge Pd_1 to catalytically-competent PdNPs (Figure 1). Very few of these studies examine Pd_n clusters stabilized by a strong 2-electron donor ligand such as XPh_3 (X = P or As).[6] Thus, we hypothesize that Pd_n cluster species that bridge Pd_1 species to PdNPs could be competent Pd catalysts, particularly those that form on reduction of a standard Pd^{II} precatalyst system, which are typically employed in chemical synthesis laboratories. This 'Pd_n cluster' hypothesis is built on a strong foundation, as well-defined triangular $[Pd_3(\mu^2\text{-}X)(\mu^2\text{-}PPh_2)_2(PPh_3)_3][SbF_6]$ clusters can mediate Suzuki-Miyaura cross-coupling (SMCC) reactions,[7a] apparently inverting the order of steps within the catalytic cycle, which links to other interesting observations made in cross-coupling reactions.[7b,7c] Noteworthy studies by Mastri, Malacria and co-workers have examined related cyclic Pd_3 clusters in the semi-hydrogenation of alkynes to alkenes and cycloisomerization reactions.[8] Furthermore, Fairlamb *et al.* reported in 2019 that $[Pd_3(\mu^2\text{-}Y)(PPh_3)_3(\mu^2\text{-}PPh_2)_2]Y$ clusters (Y = halide or acetate) are formed from a $Pd(OAc)_2/2PPh_3$ pre-catalyst system in the presence of organohalides, which were also found to be catalytically competent SMCC catalysts.[9]

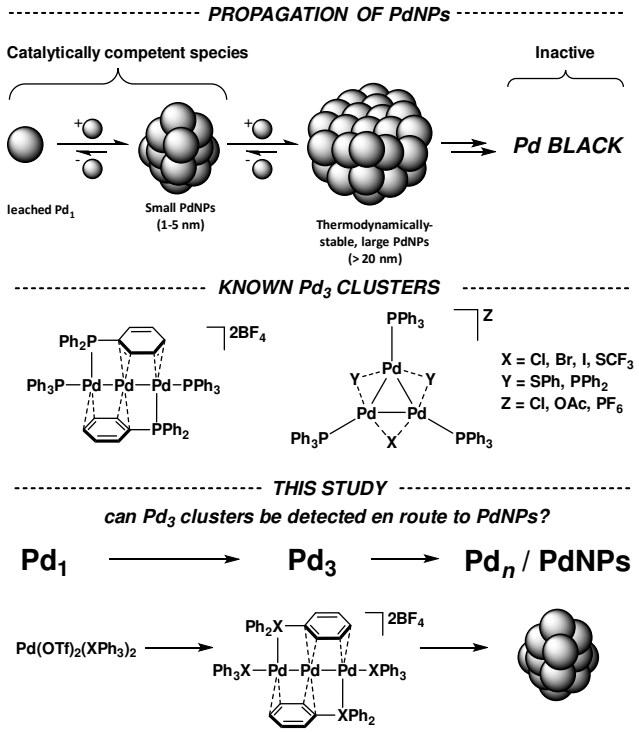

Figure 1: Top: Schematic of the equilibrium between Pd monomers and PdNPs. Middle: Known Pd_3 type clusters. Bottom: simplified representation connecting Pd_3-type clusters with PdNPs, derived from suitable Pd^{II} precursor complexes.

On the other hand, linear $[Pd_3(PPh_3)_4][BF_4]_2$ clusters have been reported in the literature as unusual entities derived from non-traditional Pd^{II} precursor complexes such as $[Pd(\mu\text{-}OH)(PPh_3)_2]_2[BF_4]_2$.[10] The competency of linear $[Pd_3(PPh_3)_4][BF_4]_2$ in cross-coupling catalysis is largely unknown. Furthermore it is unclear whether linear $[Pd_3(PPh_3)_4][X]_2$ clusters can form from more traditional mononuclear Pd^{II} phosphine precursor complexes, as is the case for cyclic $[Pd_3(\mu^2\text{-}Y)(\mu^2\text{-}PPh_2)_2(PPh_3)_3]Y$ clusters.[11] Thus, we were interested in identifying suitable mononuclear Pd^{II} precursor complexes having the potential to generate intermediate Pd_n clusters, that provide a bridge to PdNPs. We hypothesized that linear $[Pd_3(XPh_3)_4][OTf]_2$ clusters could derive from suitable $Pd(OTf)_2(XPh_3)_2$ complexes upon hydrogenation, based on previous literature precedent (where X = P).[12,13] The linear arrangement of such $[Pd_3(XPh_3)_4][OTf]_2$ clusters could serve as an ideal stationary point *en route* to PdNPs, formed by ligand loss, Pd reduction and Pd aggregation. In this context it is pertinent to mention the studies reported by Omondi *et al.* who formed $[Pd_2\{(PPh_3)(OTf)\}_2].CH_2Cl_2$, $[Pd_3\{(PPh_3)\}[OTf)_2]$ and $[Pd_3(PPh_3)_4][OTf]_2$ from the reaction of $Pd(OAc)_2$ with $2PPh_3$ in the presence of triflic acid (the latter cluster requiring MeOH).[14] † Only one of these, $[Pd_3(PPh_3)_4][OTf]_2$, was characterized by NMR spectroscopic analysis. Unfortunately, an unknown impurity at *ca.* δ_P 37 ppm accompanied $[Pd_3(PPh_3)_4][OTf]_2$.‡

Establishing a clear pathway that connects Pd_1, *via* small Pd_n clusters stabilized by 2-electron donor ligands, to PdNPs would represent a breakthrough in understanding the process wherein highly-ordered PdNPs form from 'simple' mononuclear Pd^{II} precursor complexes, while also enabling the catalytic performance of the intermediates, and well-defined Pd_n clusters, to be examined in relevant and applied catalytic chemistry. We herein describe our findings.

Results and Discussion

We expected the mononuclear Pd^{II} complexes, $Pd(OTf)_2(XPh_3)_2$ (X = P or As), to be highly amenable to mild reduction to Pd^0, having two highly electron-withdrawing ligands configured in a *cis*-geometry. Curiously, within the literature very little is known about the propensity of such species to generate Pd^0 species, whether they be mononuclear or higher order species. Generally, the soft $AsPh_3$ ligand is used as a stabilizing ligand in Pd-catalysed cross-coupling reactions, particularly Stille couplings,[15] which is the reason for its inclusion for comparison with the more ubiquitous PPh_3 ligand here. Thus, two Pd^{II} mononuclear complexes, *cis*-$[Pd(OTf)_2(PPh_3)_2]$ and *cis*-$[Pd(OTf)_2(AsPh_3)_2]$, were prepared by reported procedures.[16]

As H_2 is a mild reducing agent, the reduction of the *cis*-$[Pd(OTf)_2(XPh_3)_2]$ complexes was examined by charging degassed CH_2Cl_2 solutions (7.6 mM) with H_2 (3 bar) in a Young's NMR tube at room temperature. The solutions gradually darkened from transparent yellow, due to the formation of new hydrido-containing Pd^{II} species (*vide infra*), to translucent red/brown. These color changes qualitatively indicate a change from P^{II} to Pd^0, and the formation of colloidal PdNPs, which is typically brown to dark brown in color (note: a black coloration and appearance of black particles visible to the naked eye, >10 μm in size, are associated with formation of inactive *Pd Black*, Fig. 1). The red coloration indicates that soluble molecular Pd species are present (*vide infra*).

Firstly, we characterized the PdNPs derived from *cis*-$[Pd(OTf)_2(PPh_3)_2]$ and *cis*-$[Pd(OTf)_2(AsPh_3)_2]$ by transmission electron microscopy (TEM, Fig. 2), and have hitherto described characterization of PdNPs formed under reductive reaction conditions by TEM.[17] As the TEM grid method requires evaporation of Pd solutions *in vacuo*, we employed a known PdNP stabilizer, polyvinylpyrrolidone (PVP) which prevents Pd aggregation *in vacuo*. Samples were thus examined in the presence and absence of PVP.[18] The method showed no discernible change in the size of the PdNPs formed from *cis*-$[Pd(OTf)_2(XPh_3)_2]$ (X = P, As) *ex situ*, in the presence or absence of stabilizing PVP polymer. The TEM images reveal a uniform distribution of PdNPs derived from both *cis*-$[Pd(OTf)_2(XPh_3)_2]$ complexes, which are likely stabilized by the XPh_3 ligands (Fig. 2). PdNPs stabilized by PPh_3 ligands, of similar size and shape to those imaged here (*i.e.* spherical truncated icosahedra[19]), have been independently reported.[20]

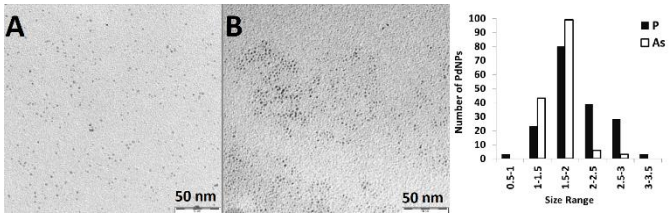

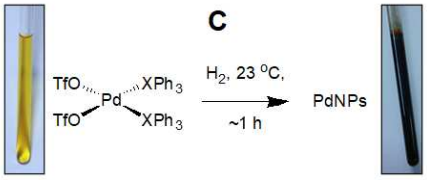

Figure 2: Histogram data comparing PdNP size distribution that form on addition of hydrogen to $[Pd(OTf)_2(PPh_3)_2]$ (**A**) and $[Pd(OTf)_2(AsPh_3)_2]$ (**B**). Mean size (Std. Dev.): X = P 1.98 nm (0.46 nm); X =As 1.70 (0.32). The image in **C** shows the colour changes seen on converting $[Pd(OTf)_2(PPh_3)_2]$ to PdNPs (representative example X = P or As).

The calculated size distributions of the PdNPs (Fig. 2) range from 1 to 4 nm, with no discernible difference between the mean sizes of those that form from addition of H_2 to *cis*-$[Pd(OTf)_2(PPh_3)_2]$ and *cis*-$Pd(OTf)_2(AsPh_3)_2$. The similarity of these small PdNPs to those previously reported indicate the potential for catalyst activity in cross-coupling reactions (*vide infra*).[21] Critically, observation that PdNPs form confirms the hypothesis that *cis*-$[Pd(OTf)_2(XR_3)_2]$ are viable Pd^{II} precursor salts for further catalytic study.

Detection of hydrido-Pd^{II} complexes en route to higher order Pd species: NMR spectroscopic analysis enabled investigation of the potential pathways taken by *cis*-$[Pd(OTf)_2(XPh_3)_2]$, on exposure to H_2, en route to forming PdNPs. Upon addition of H_2 gas (3 bar), the formation of PdNPs leads to the liberation of free XPh_3 ligands (observed in solution by ^1H NMR, with PPh_3 seen by ^{31}P NMR). Critically, several new 'Pd^{II}-H' species also form (Scheme 1). Their full characterization data is given in the Supporting Information, with the key data summarized in Scheme 1. Hydride signals corresponding to *trans*-$[Pd(H)(OTf)(XPh_3)_2]$, *trans*-$[Pd(H)(XPh_3)_3][OTf]$, *trans*-$[Pd(H)(Cl_2CD_2)(XPh_3)_2]$, and *trans*-$[Pd(Cl)(H)(XPh_3)_2]$ were seen. Over time, these species reduce in concentration, and their signals eventually disappear from the associated ^1H NMR spectra. The hydride signals corresponding to *trans*-$[Pd(Cl)(H)(XPh_3)_2]$ remain visible by ^1H NMR for a longer time period than the other hydride signals. This confirms that under these conditions, *trans*-$[Pd(Cl)(H)(XPh_3)_2]$ is the most thermally stable monohydride Pd^{II} species in solution. Concomitant with the formation of *trans*-$[Pd(Cl)(H)(XPh_3)_2]$ is the formation of TfOH and $[HXPh_3]^+$, and an unusual new species as noted by monitoring the evolution of ^1H NMR signals in the aromatic region (*vide infra*). Thus, the effects of the stabilizing triflate anion and XPh_3 ligands reduce over time.

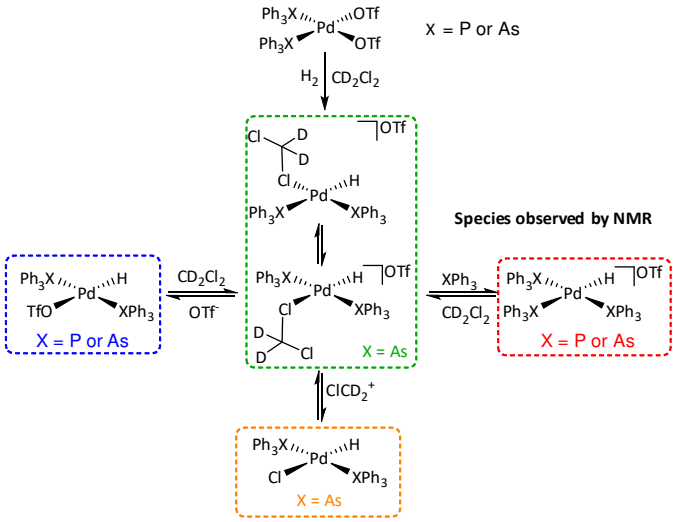

Scheme 1: Monohydride species detected by NMR and LIFDI-MS, on addition of hydrogen to d_2-dichloromethane solutions of $[Pd(OTf)_2(XPh_3)_2]$.

Detection of linear $[Pd_3(PPh_3)_4][OTf]_2$ complexes in solution: A key observation made in this study is that as the hydride NMR signals corresponding to the Pd^{II} monohydride species (Scheme 1) derived from *cis*-$[Pd(OTf)_2(XPh_3)_2]$ reduce in intensity, several unusual ^1H NMR signals appear. For *cis*-$[Pd(OTf)_2(PPh_3)_2]$, several new ^{31}P NMR signals are also detected. The most identifiable of the new NMR signals observed are shown in Fig. 3(a) for $XR_3 = PPh_3$. Although the ^1H NMR signals appear as triplets, with a 1:1 integral ratio, their chemical shifts are unusual; they correspond to the protons in PPh_3 that are shifted considerably up-field to δ 5.98 and 4.74. Up-field shifts of this type are the result of significant proton shielding by a neighboring electron-rich Pd center(s). A ^1H $\{^{31}P\}$ NMR spectrum showed that the signal at δ 5.98 is unaffected by de-coupling to phosphorus, whereas the signal at δ 4.74 collapses to a doublet. The *pseudo*-triplet splitting is therefore the result of both J_{HH} and J_{HP} couplings, characteristic of the *ortho* protons of the PPh_3 ligand. ^{31}P-optimised HMQC spectra revealed a cross-peak between the ^1H NMR signal at δ 4.74 and ^{31}P NMR signal at δ 43.53. This ^{31}P $\{^1H\}$ NMR signal is shown in Fig. 3(b), and displays an unusual AA'XX' splitting pattern,[22] [17] which is only observed if there are four magnetically inequivalent nuclear spins, consisting of two pairs of chemically equivalent nuclear spins. This Pd species must therefore contain four magnetically inequivalent phosphorus environments, but only two chemically inequivalent phosphorus environments. This is supported by a second AA'XX' ^{31}P NMR signal at δ 9.06, with the ^{31}P NMR signals having an integral ratio of 1:1.

Single crystals of $[Pd_3(PPh_3)_4][OTf]_2$ were grown from this NMR sample by layering non-dried reagent grade hexane above the d_2-dichloromethane layer, allowing the solvents to slowly diffuse. The trace water aided crystallization by forming a H-bond network with the triflate counterions (note: crystals did not form when dry hexane was used). The crystal structure was solved using single crystal X-ray diffraction methods {XRD, Fig. 3(c)}. The crystal structural data reveals three Pd atoms bonded linearly and stabilized by four PPh_3 ligands, two of which lie perfectly in the Pd-Pd-Pd plane, and two that are positioned outside of the plane.

For the latter, bridging PPh_3 ligands are coordinating to the Pd by sigma donation from phosphorus and η_2-coordination from one of the three phenyl rings, so that there are four η_2-C=C bonds stabilizing the Pd centers for the complete cluster. The complex has an overall charge of +2. The Pd-Pd bond length in the crystal structure is 2.6313(19) Å, which is marginally longer than typical Pd^I-Pd^I bond lengths,[23] thus suggesting a Pd^I-Pd^0-Pd^I type structure. The arene bonding interactions are shorter at Pd1 {C1-Pd1 = 2.1925(16) and C2-Pd1 = 2.2650(17) Å} than at Pd2 {C3-Pd2 = 2.3865(17) and C4-Pd2 = 2.2985(17) Å}, consistent with the central Pd atom being in an oxidation state of zero, with greater synergic back-bonding with the π*-antibonding orbitals of the arene. The uncoordinated C5-C6 bonds have shortened, resembling more closely an isolated C=C bond 1.374(2) Å.

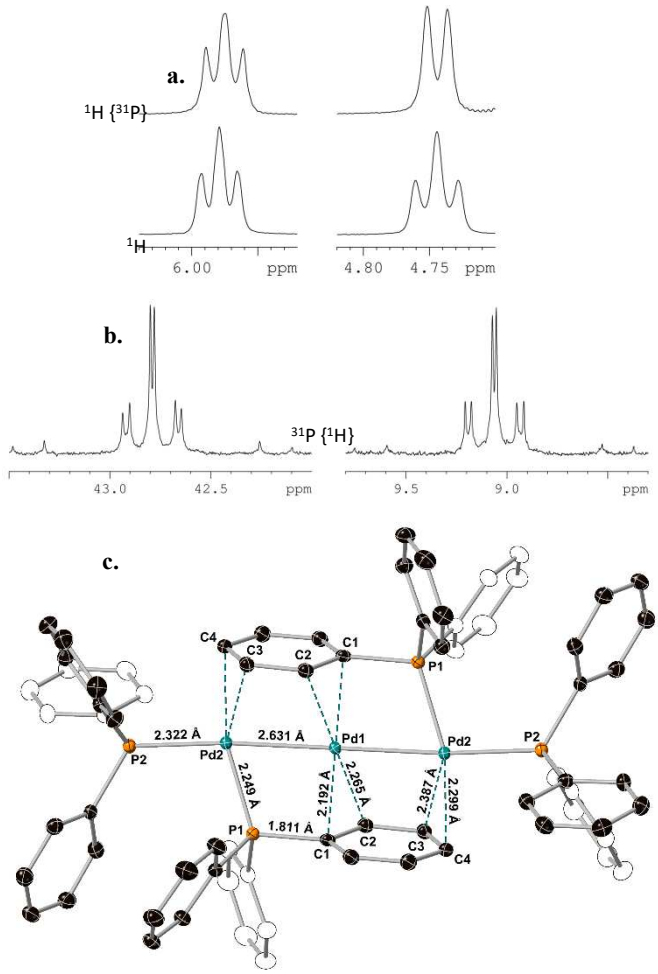

Figure 3: **a.** Unusual ^{1}H (above) and ^{1}H {^{31}P} (below) NMR signals that correspond to the protons of triphenylphosphine interacting with Pd in $[Pd_3(PPh_3)_4][OTf]_2$. **b.** ^{31}P {^{1}H} NMR signals that correspond to the phosphorus nuclei in $[Pd_3(PPh_3)_4][OTf]_2$, having an AA'XX' splitting pattern. **c.** X-ray crystal structure of $[Pd_3(PPh_3)_4][OTf]_2$; the OTf counterions, H_2O and H-atoms omitted for clarity. Thermal ellipsoids set to 50% probability.

LIFDI-MS analysis of a d_2-dichloromethane solution containing $[Pd_3(PPh_3)_4][OTf]_2$ showed an ion signal at m/z 684.54, corresponding to the dicationic tri-Pd cluster ($[M\text{-}[OTf]]^{2+}$), having a formal molecular mass of 1368.40 gmol^{-1}, which confirms that $[Pd_3(PPh_3)_4][OTf]_2$ is present both in solution and the solid-state. Overall, there is a net reduction of Pd^{II} in forming this new species.

As mentioned in the introduction, despite its unusual appearance, the linear $[Pd_3(PPh_3)_4]^{2+}$ cluster is a known dication, stabilized by tetrafluoroborate rather than triflate.[10] It was previously formed by adding ethanol (a necessary requirement) to a dichloromethane solution of $[Pd(\mu\text{-}OH)(PPh_3)_2]_2[BF_4]_2$.[9] The η^2,η^2-coordination of PPh_3 to Pd is unique to $[Pd_3(PPh_3)_4]^{2+}$, although η^1-coordination from the *ipso*-carbon atoms are known in a dinuclear Pd complex.[24] Furthermore, the handful of dinuclear Pd^I complexes that are stabilized *via* η-coordination of bridging arenes do not form as reaction intermediates, but have been synthesized either as (pre)catalysts for cross-coupling reactions, or as complexes that are interesting in their own right.[25] Longer, linear Pd clusters stabilized by η^2-C=C coordination from polyenes are known.[26] Interestingly, Pd^I species containing bridging arenes from the more complicated and apparently robust phosphine ligands such as X-Phos and S-Phos have been reported in the recent literature, but again the implications for catalysis have not been fully delineated.[27]

The diagnostic ^{1}H and ^{31}P{^{1}H} NMR signals of $[Pd_3(PPh_3)_4][OTf]_2$ are given in the ESI. Coupling between the phosphorus nuclei that are positioned *trans* to one another ($J_{XX'}$) is very strong (~ 98 Hz), despite this being a 4-bond coupling. As expected, coupling between the phosphorus nuclei that are positioned *cis* to one another (J_{AX} ~ 35 Hz) is stronger than the coupling between the more remote AX' phosphines ($J_{AX'}$ ~ 9 Hz). The coupling constants between the ^{31}P nuclei of the Pd_3 complex support a similar structure in solution as in the solid-state. The η^2-C=C coordination to Pd from the phenyl rings (x4) restrict the geometry upon complexation.

In keeping with the characterization of $[Pd_3(PPh_3)_4][OTf]_2$, ^{1}H NMR signals for $[Pd_3(AsPh_3)_4][OTf]_2$ deriving from *cis*-$Pd(OTf)_2(AsPh_3)_2$ are similar in appearance and chemical shift. The XRD crystal structure of $[Pd_3(AsPh_3)_4][OTf]_2$ was also obtained (Fig. 4), which co-crystallizes with two equivalents of triflic acid. The equivalence of the phenyl groups in these $AsPh_3$ ligands leads to the η^2,η^2-coordinated phenyl rings having two equivalent *ortho* and two equivalent *meta* protons. As with $[Pd_3(PPh_3)_4][OTf]_2$, η^2,η^2-coordination of the phenyl rings results in a weakening of the π-bonds, resulting in longer C-C bond lengths. Experimental m/z values, with matching simulated isotope distribution patterns, confirm that $[Pd_3(AsPh_3)_4][OTf]_2$ is present in solution, as in the solid-state.

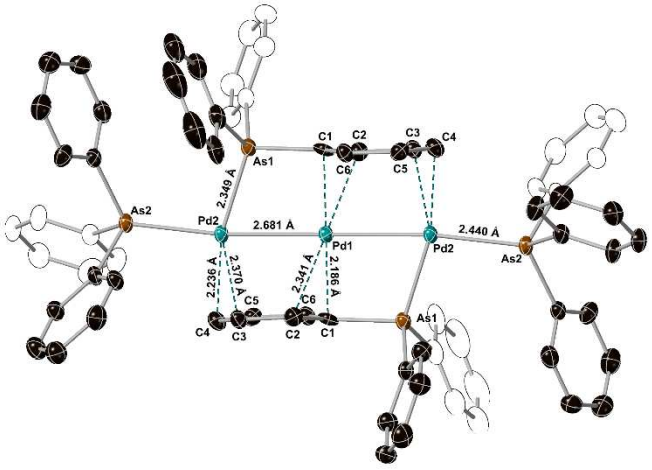

Figure 4: X-ray crystal structure of $[Pd_3(AsPh_3)_4][OTf]_2$. Two triflate counterions, two triflic acid molecules and the H-atoms have been omitted for clarity. Thermal ellipsoids set to 50% probability.

Photoisomerization properties of $[Pd_3(XPh_3)_4]^{2+}$. The $[Pd_3(XPh_3)_4]^{2+}$ species form brightly colored solutions, ranging from yellow to red in color. This is due to absorption bands in the visible region of the EM spectrum. The UV-vis absorption spectra of $[Pd_3(PPh_3)_4][OTf]_2$ and $[Pd_3(AsPh_3)_4][OTf]_2$ are given in Fig. 5. Their respective molar absorption coefficients at λmax were calculated to be $3.7x10^4$ and $4.7x10^4$ mol-1dm^{3}cm^{-1}, which are too large to correspond to Laporte forbidden d-d transitions, suggesting the presence of charge transfer (CT) bands and potential photoactivity.

We focused photoactivation studies on $[Pd_3(PPh_3)_4][BF_4]_2$, as practically it was easier than $[Pd_3(PPh_3)_4][OTf]_2$ to access larger quantities in pure form. It is important to note that $[Pd_3(PPh_3)_4][BF_4]_2$ does degrades in solution, at temperatures as low as -85 oC. However, it is stable in the solid-state. The synthesis of $[Pd_3(PPh_3)_4][BF_4]_2$ was accomplished using the method of Sharp *et al*, for which the ratio of ethanol to CH_2Cl_2 and presence of air appears to be critically important.[10] UV irradiation of d_2-dichloromethane solutions of $[Pd_3(PPh_3)_4][BF_4]_2$ (2.16 mM) at 250 K under N_2 for 3 h led to a color change from orange/red to pink/purple. Spectral changes were noted by UV-vis absorption and NMR spectroscopic analysis for solutions before and after photoirradiation (Figs. 6 and 7). The molar absorption coefficient at λ_{max} of the solution after irradiation was calculated to be $3.05x10^4$ mol^{-1}dm^{3}cm^{-1}, corresponding again to a CT band, confirming a chemical change upon UV irradiation.

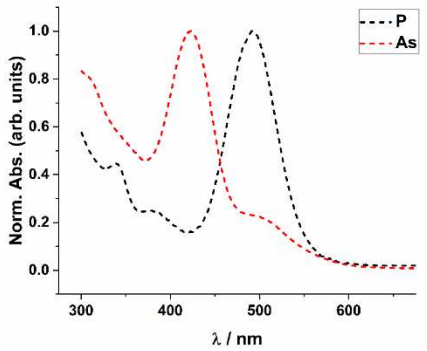

Figure 5: Normalized UV-vis absorption spectra of dichloromethane solutions of $[Pd_3(PPh_3)_4][OTf]_2$ (P) and $[Pd_3(AsPh_3)_4][OTf]_2$ (As).

^{1}H NMR spectroscopic analysis confirmed quantitative conversion of the thermal isomer to a new photoactivated species that possesses a similar chemical structure (Fig. 6). Two up-field signals, corresponding to the *ortho* and *meta* protons of the η^2-C=C coordinated phenyl rings remain, although the *ortho* signal now lies at δ 5.18 and the *meta* lies at δ 5.88. The broad *ortho* signal simplifies to a sharp doublet upon {^{31}P}-decoupling.

The ^{31}P {^{1}H} NMR spectrum of a d_2-dichloromethane solution of $[Pd_3(PPh_3)_4][BF_4]_2$, following broadband UV irradiation, is shown in Fig. 6. There are three phosphorus environments, rather than the two AA'XX' environments observed prior to irradiation, thus the symmetry of two of the original PPh_3 ligands has been lost in the photoproduct. An integral ratio at δ_P 35.69 was determined to be two, whereas the two signals at δ_P 12.41 and δ_P 10.59 were one each. Thus, the new species possesses four PPh_3 ligand environments, two of which are chemically equivalent. Furthermore, the two signals at δ 12.41 and 10.59 exhibit a second order pattern. The chemical shift difference is equal to ~300 Hz, and the *J* coupling between these signals is ~100 Hz.

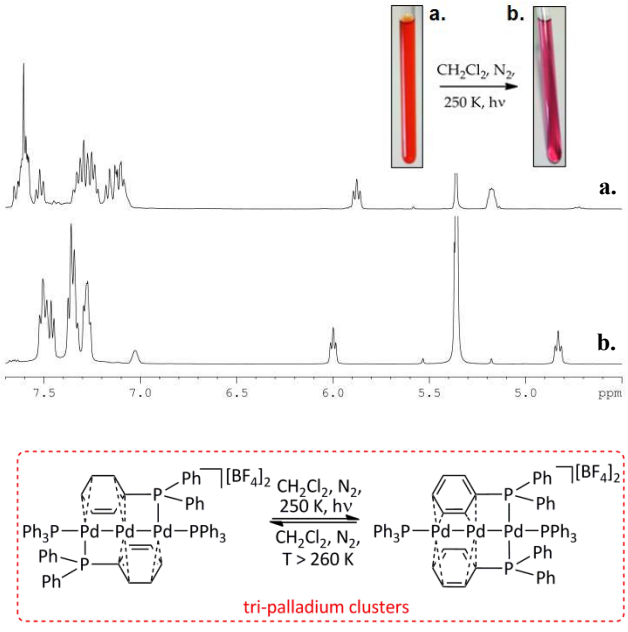

Figure 6: ^{1}H NMR spectra of d_2-dichloromethane solutions of $[Pd_3(PPh_3)_4][BF_4]_2$ after broad-band UV irradiation (a.) and before UV irradiation (b.) (the residual $CDHCl_2$ solvent peak is shown off-

scale in both spectra). The chemical change involved is described in the scheme.

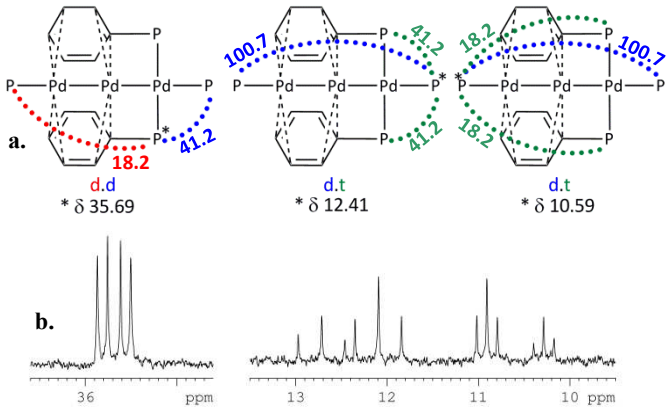

Figure 7: (a.) Schematic showing the J_{PP} coupling network that gives rise to the ^{31}P splitting patterns shown in (b.). (b.) ^{31}P {^{1}H} NMR spectrum of a d_2-dichloromethane solution of $[Pd_3(PPh_3)_4][BF_4]_2$ after UV irradiation.

^{31}P-optimised HMQC NMR spectra exhibit cross-peaks between the ^{1}H NMR signal corresponding to the *ortho* protons of the η^2-coordinated phenyls at δ 5.18 and the ^{31}P NMR signal at δ 35.69. This corresponds to the phosphorus nuclei of the phosphines that are η^2-coordinated to the Pd. This signal is a doublet of doublets, with *cis* J_{PP} couplings of 41.2 and 18.2 Hz. The coupling values suggest that these phosphorus nuclei are positioned closer to one of the two other phosphines, as shown in Fig. 7. The ^{31}P NMR signals at δ 12.41 and 10.59 are both a doublet of triplets, which share a large *trans*-coupling value of 100.7 Hz. The former signal also exhibits a *cis*-coupling of 41.2 Hz, whilst the latter signal exhibits a *cis* coupling of 18.2 Hz. As no cross peaks were observed between these up-field phosphorus NMR signals and the up-field proton NMR signals of the η^2-coordinated phenyl moieties, they likely correspond to terminal phosphines on a linear Pd complex, which matches with their mutual *trans*-coupling (Fig. 7).

Using LIFDI-MS to probe the species in solution, the only signal observed appeared at *m/z* 683.6, which is identical to the *m/z* of the dicationic tri-Pd cluster $[Pd_3(PPh_3)_4]^{2+}$. This confirms that the new Pd species that forms on irradiation of the d_2-dichloromethane solution of $[Pd_3(PPh_3)_4][BF_4]_2$ is a photoisomer. A single crystal was grown from the d_2-dichloromethane solution of the photoisomer $[Pd_3(PPh_3)_4][BF_4]_2$ by layering with dry hexane −20 °C. The XRD crystal structure is shown in Fig. 8.

The three Pd atoms are again bonded linearly with the terminal phosphines lying in the plane. Unlike the thermal isomeric form of $[Pd_3(PPh_3)_4]^{2+}$, the Pd atoms are not perfectly linear; there is a slight bend out of plane so that the Pd-Pd-Pd angle is 171.26°. As with the thermal isomer, the two η^2-coordinated phenyl rings enablie stabilization of the linearly arranged Pd atoms. There is an unsymmetrical coordination of both phenyl groups, and the bonding interactions are stronger for the photoisomeric form of $[Pd_3(PPh_3)_4]^{2+}$.

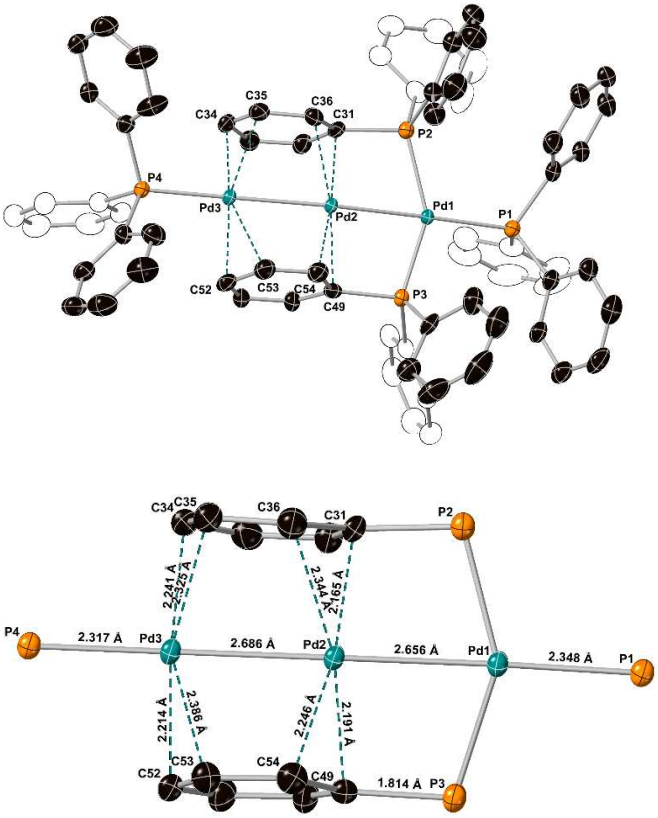

Figure 8: Top: X-ray crystal structure of the $[Pd_3(PPh_3)_4][BF_4]_2$ photoisomer, formed on UV irradiation of d_2-dichloromethane solutions of $[Pd_3(PPh_3)_4][BF_4]_2$; Bottom: a truncated view with key bond distances shown. The BF_4 counterions, solvent molecules and H-atoms have been omitted for clarity. Thermal ellipsoids set to 50% probability.

The photoisomerization of $[Pd_3(PPh_3)_4][BF_4]_2$ (1.08 mM) in d_2-dichloromethane solution with a 200 W broadband UV source, proceeds at an effective rate of 5.47×10^{-5} s^{-1} ± 5×10^{-8} s^{-1} at 240 K. This data was determined through ^{1}H NMR spectroscopy with *in situ* irradiation.[28] No evidence for the reformation of the thermal isomer is observed at 240 K, however at room temperature (298 K), equilibration based on reversible isomerization occurs over several days.

Computational studies using density functional theory (DFT) methods were used to probe the electronic structure of the thermal and photoisomeric forms of $[Pd_3(PPh_3)_4]^{2+}$ (Fig. 9). The geometries were optimized initially using a B3LYP functional and def2svp basis set, applied with Grimme's empirical dispersion correction (GD3), using a CH_2Cl_2 implicit solvent model (cpcm model, using Gaussian 16 Rev. A.03 Win64). Time-dependent DFT calculations were then conducted, using a cam-b3lyp[29] functional and def2svp basis set (50 states). The calculations were in good agreement with the experimental UV-vis spectral data collected for the thermal and photoisomeric forms of $[Pd_3(PPh_3)_4][OTf]_2$ (in CH_2Cl_2). For both thermal and photoisomeric forms we see that the lowest energy transition is dominated primarily by the $HOMO_{(302)}$/$LUMO_{(303)}$ interaction (with oscillator strengths of 1.1352 and 0.9262 in the thermal and photochemical isomeric forms of $[Pd_3(PPh_3)_4]^{2+}$ respectively). The HO-

MOs are localized on the terminal Pd atoms into the donor co-ordinated arenes. The LUMO are localized across the three bridging Pd atoms, involving P and the coordinated bridging arene moieties. We also observe a small contribution to the major transition in the photoisomeric form of $[Pd_3(PPh_3)_4]^{2+}$ from HOMO-5$_{(297)}$ to LUMO$_{(303)}$. The thermal isomer of $[Pd_3(PPh_3)_4]^{2+}$ has a lower sum of thermal and electronic free energy than the photochemical isomer by 5.4 kcal/mol.

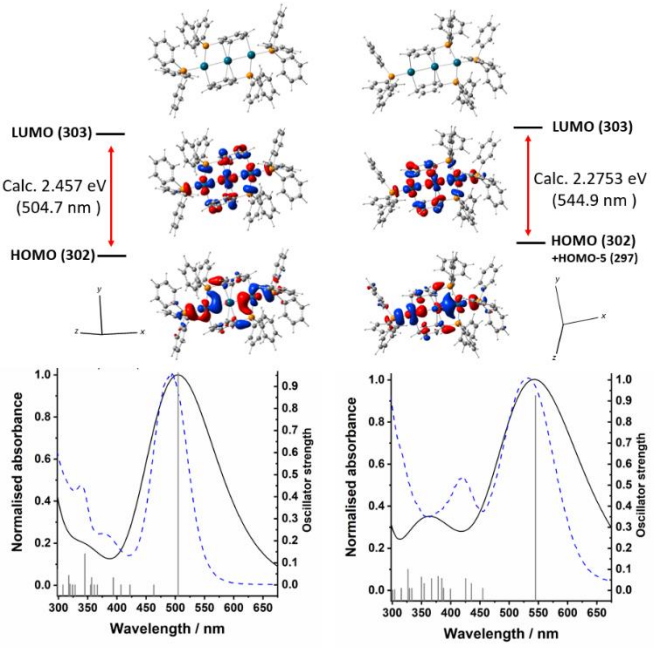

Figure 9: Computed structures of the thermal and photoisomeric forms of $[Pd_3(PPh_3)_4]^{2+}$, compared with the experimental UV-vis spectral data (blue dashed line) for the thermal and photoisomeric forms of $[Pd_3(PPh_3)_4][OTf]_2$ in CH_2Cl_2.

Catalytic Competency of $[Pd_3(PPh_3)_4]^{2+}$ species

As we have established that the $[Pd_3(XPh_3)_4][OTf]_2$ complexes form as intermediates during the transition of mononuclear Pd complexes to PdNPs, we expected to see a role for them in catalysis, particularly as it has been demonstrated that cyclic triangular Pd_3 clusters are active cross-coupling catalysts.[7a] We therefore examined the catalytic competency of the linear $[Pd_3(XPh_3)_4]^{2+}$ species, and due to the ease of synthesis and isolation, we focused on the use of the thermal isomer of $[Pd_3(PPh_3)_4][BF_4]_2$.

The catalytic competency of $[Pd_3(PPh_3)_4][BF_4]_2$ (thermal isomer) was next assessed in a C-C bond-forming reaction, namely the SMCC reaction of 4-bromo-6-methyl-2-pyrone **1** with 4-methylphenylboronic acid **2a** to form 6-methyl-4-(*p*-tolyl)-2-pyrone **3** – this reaction is a good test as the 2-pyrone heterocycle can readily undergo side-reactions (Fig. 10). The conditions {THF/H_2O (biphasic), 2M Na_2CO_3, 50 ºC for 4 h} used for the SMCC catalyst screening are typical.[30] The activity of $[Pd_3(PPh_3)_4][BF_4]_2$ was compared to that of freshly-prepared $[Pd(PPh_3)_4]$, as the most commonly-used Pd catalyst for SMCC reactions.[31] The Pd^{II} precursor complex, $[Pd(OTf)_2(PPh_3)_2]$, which forms $[Pd_3(PPh_3)_4][OTf]_2$ on reduction with H_2 *vide supra*, was also compared as a secondary benchmark (precatalyst). Product conversions were measured by ^{1}H NMR reaction monitoring of crude product mixtures. The percentage conversions and yields of isolated product **3**, synthesized using different Pd catalysts, are collated in Table 1. Surprisingly, the lowest conversion was obtained using freshly prepared $[Pd(PPh_3)_4]$ (44%, isolated yield 42%). The highest conversion of 85% and yield of 80% was obtained employing the thermal isomeric form of $[Pd_3(PPh_3)_4][BF_4]_2$ (0.33 mol% catalyst loading). We noted that the THF layer (biphasic mixture with water) changed color from a bright red transparent solution to a dark brown translucent solution; Pd black was deposited on the reaction glass vessel on complete loss of **1**.

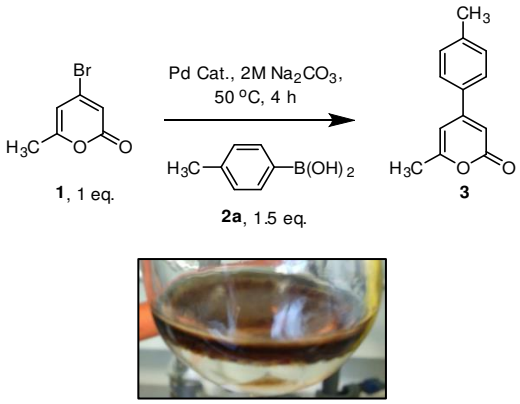

Figure 10: SMCC reaction of 4-bromo-6-methyl-2-pyrone **1** with 4-methylphenylboronic acid **2a** to form 6-methyl-4-(*p*-tolyl)-2-pyrone. The image shows the reaction catalyzed by $[Pd_3(PPh_3)_4][BF_4]_2$ where the PdNPs that form appear to remain in the upper THF solvent layer upon reaction completion.

Table 1: Percentage conversion (NMR) and percentage yields of isolated 6-methyl-4-(4-methylphenyl)-2-pyrone 3, on cross-coupling 4-bromo-6-methyl-2-pyrone 1 with 4-methylphenylboronic acid 2, using Pd catalysts stated.

Catalyst	Mol% Cat.	Conv. by NMR (%)	Isolated yield of **3** (%)
$[Pd(PPh_3)_4$	1	44	42
$[Pd(OTf)_2(PPh_3)_2]$	1	77	76
$[Pd_3(PPh_3)_4][BF_4]_2$	1	80	76
$[Pd_3(PPh_3)_4][BF_4]_2$	0.33	85	80

The ^{1}H NMR spectra that were subsequently acquired did not contain any of the proton signals corresponding to $[Pd_3(PPh_3)_4][BF_4]_2$. The high conversions achieved using $[Pd_3(PPh_3)_4][BF_4]_2$ confirm that, even under the mild conditions used here, the tri-Pd complex reacts further to form the active catalytic species, *i.e.* agglomerated PdNPs.[32,33] A high percentage conversion of 77% was obtained using $[Pd(OTf)_2(PPh_3)_2]$, with an isolated yield of 76% recorded for product **3**. As with $[Pd_3(PPh_3)_4][BF_4]_2$, the THF layer was observed to change color during the SMCC reaction, from an orange/yellow transparent solution to a dark brown translucent solution, after which time Pd black was deposited on the reaction glass vessel on complete loss of **1**.

These initial studies point toward PdNPs being the destination for the Pd species formed under the catalytic SMCC conditions detailed above. In 2021, we uncovered that related cyclic Pd_3 clusters and stabilized PdNPs (generated *in situ*) exhibit different catalyst behavior in SMCC reactions of 2,4-dibromopyridine **4** with organometallic reagents to give arylated pyridine products

(Figure 11, **A**).[34] Typically, mononuclear Pd catalysts such as $[Pd(PPh_3)_4]$ exhibit high selectivity for the C2-arylation product ($\mathbf{5}_{C2Ar}$) over the C4-arylation product ($\mathbf{5}_{C4Ar}$).[35] As a specific example we found that reaction of **4** with aryl boronic acid **2b** promoted a switch in site-selectivity from C2 to C4 ($\mathbf{5}_{C4Ar}$ being the dominate product) when using either a precatalyst system made of $Pd(OAc)_2$/<2PPh_3 or the cyclic trinuclear Pd cluster $[Pd_3(\mu^2\text{-}Cl)(\mu^2\text{-}PPh_2)_2(PPh_3)_3]Cl$ (Figure 11, **B**). The diarylation product **6** is a common (competing) side-product. Our mechanistic work showed that the site-selectivity switch was associated with being able to access Pd clusters and PdNPs under the reaction conditions. Thus, the SMCC reaction represents an excellent testing ground for assessing the catalyst behavior and speciation deriving from $[Pd_3(PPh_3)_4][BF_4]_2$.

Under our optimized conditions, note fully homogeneous, we found that 1 mol% of $[Pd_3(PPh_3)_4][BF_4]_2$ (thermal isomer) was highly effective at promoting the SMCC reaction, with the reaction depleted of the limiting reagent (**4**) within 30 minutes. Crucially, high C4-selectivity was seen for $\mathbf{5}_{C4Ar}$ showing that $[Pd_3(PPh_3)_4][BF_4]_2$ behaves similarly to $[Pd_3(\mu^2\text{-}Cl)(\mu^2\text{-}PPh_2)_2(PPh_3)_3]Cl$ and higher order PdNPs in this reaction. After 30 minutes we noticed some loss of $\mathbf{5}_{C4Ar}$ which serves as a reactive substrate for reaction with excess **2b** to give diarylated product **6**.

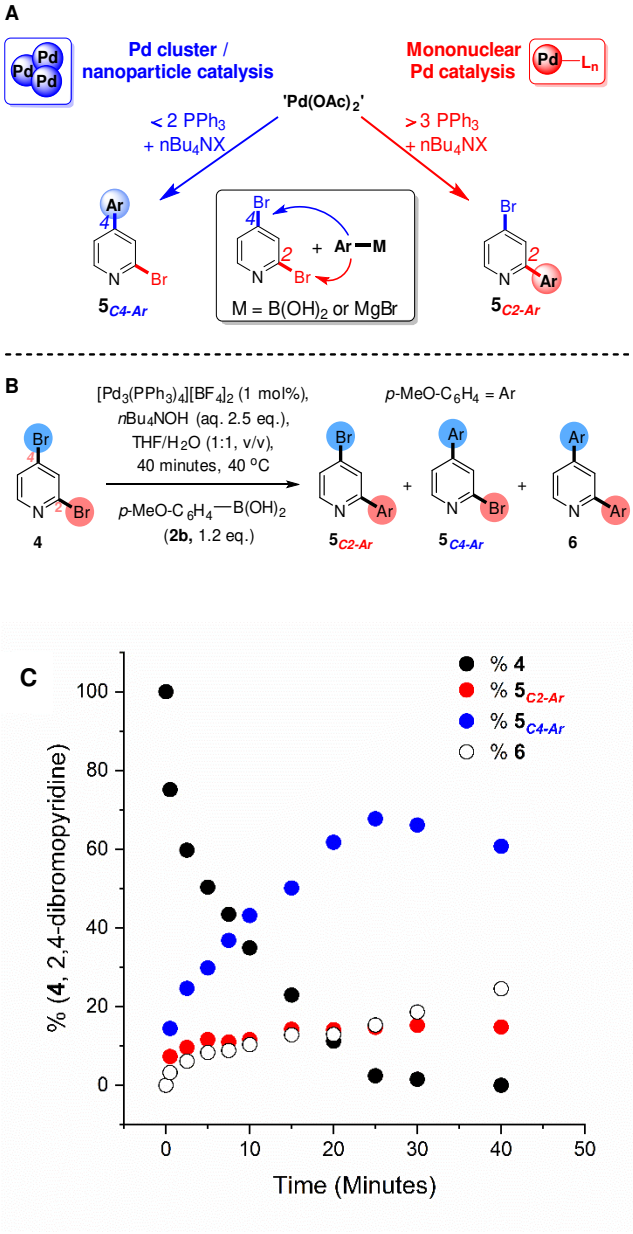

Figure 11: **A** Behavior of Pd catalyst species in the cross-coupling reactions of 2,4-dibromopyridine **4** with organometallic reagents. **B** SMCC reaction of **4** with 4-methoxyphenylboronic acid **2b** to form monoarylated products $\mathbf{5}_{C2Ar}$ and $\mathbf{5}_{C4Ar}$ and diarylated product **6**. **C** kinetic behavior of the SMCC reaction of **4** with **2b** catalyzed by 1 mol% $[Pd_3(PPh_3)_4][BF_4]_2$.

Lastly, we have determined that both thermal and photoisomers of $[Pd_3(XPh_3)_4]^{2+}$ are similarly catalytically active in the Pd-catalyzed hydrogenation of phenylacetylene to give styrene (see Supporting Information for further details).

Conclusions

Addition of hydrogen to d_2-dichloromethane solutions of $[Pd(OTf)_2(XPh_3)_2]$ complexes (X = As and P) led to the formation of Pd^{II} monohydride species (Fig. 12). Over time, NMR signals corresponding to linear $[Pd_3(XPh_3)_4][OTf]_2$ were found to grow in intensity, and these proved thermodynamically stable and isolable. These species have been characterized by NMR, LIFDI-MS,

and single-crystal XRD. They are unusual in so far as the Pd atoms are stabilized by η^2-coordination from the phenyl rings of the phosphine or arsine ligands, which results in a loss of ring aromaticity. Such η^2-coordination of phenyl rings directly bound to both phosphorus- and arsenic-containing ligands is rare and undoubtedly makes them a suitable catalyst precursor that are activated at just 40 ºC. The overall charge of these $[Pd_3(XPh_3)_4][OTf]_2$ species is +2. Thus, the Pd^{II} mononuclear complex has been reduced so that each Pd atom now has an average oxidation state of +2/3. Formally though, the cluster is a reservoir of both Pd^{II} and Pd^0 species. This facile reduction of Pd(II) suggests that the $[Pd_3(XPh_3)_4][OTf]_2$ complexes reflect stable resting states that form *en route* to PdNPs, the latter of which have been characterized by TEM analysis.

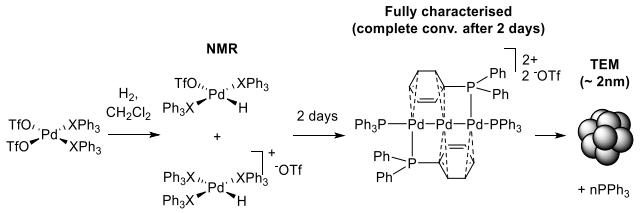

Figure 12: Schematic to show pathway to higher order Pd species, involving the intermediate formation of $[Pd_3(PPh_3)_4][BF_4]_2$.

Interestingly, reducing $[Pd(OTf)_2(XPh_3)_2]$ complexes with H_2 provides a novel means for accessing the $[Pd_3(XPh_3)_4][OTf]_2$ species. As we have demonstrated that these species form with commonly used PPh_3 and $AsPh_3$ ligands, it is possible that they form in a range of Pd-catalyzed reactions. They could therefore reflect active catalysts, or conduits to active catalysts such as PdNPs and/or other Pd_n clusters.

The $[Pd_3(XPh_3)_4]^{2+}$ species form brightly colored solutions due to CT electronic transitions which give rise to large molar absorption coefficients in the visible spectral region. Irradiation of $[Pd_3(PPh_3)_4][BF_4]_2$ with broadband UV light resulted in photoisomerization to a novel and unusual higher energy photoisomeric form, which was characterized by NMR, LIFDI-MS, and single-crystal XRD. The dynamic behavior of the PPh_3 ligand in a linear Pd_3 cluster arrangement has been evidenced, showing that this simple and ubiquitous ligand continues to exhibit new information about its rich coordination chemistry.

Both the thermal and photoisomeric forms of $[Pd_3(PPh_3)_4][BF_4]_2$ are catalytically competent in two separate SMCC reactions. From the experimental evidence we conclude that $[Pd_3(PPh_3)_4][BF_4]_2$ forms an active Pd catalyst species, most likely PdNPs (as characterized by TEM *vide supra*), which bring about a switch in site-selectivity from C2 to C4 in SMCC reactions of 2,4-dibromopyridine, highlighting that these aggregated Pd species can also alter expected catalytic reaction outcomes. We are currently examining potential links between the formation of linear $[Pd_3(PPh_3)_4]^{2+}$ and cyclic $[Pd_3(\mu^2\text{-}X)(PPh_3)_3(\mu^2\text{-}PPh_2)_2]^+$ clusters.[6,7,9]

Notes

† We found that the reaction of $Pd(OAc)_2$ with $2PPh_3$ in THF forms *trans*-$Pd(OAc)_2(PPh_3)_2$ initially. This converts to an alternative dinuclear Pd^I complex, which subsequently reacts with CH_2Cl_2 to form triangular Pd_3 cyclic clusters.[9]

‡ We have also detected the formation of a similar unknown impurity in the synthesis of $[Pd_3(PPh_3)_4][BF_4]_2$ reported by Sharp *et al.*[10] which is formed in varying amounts and has to be removed by careful crystallization.

ASSOCIATED CONTENT

Supporting Information

Included within a PDF file is the full synthetic procedures and compound characterization data, catalysis experiments and NMR studies. The Supporting Information is available free of charge on the ACS Publications website.

AUTHOR INFORMATION

Corresponding Author

Joint corresponding authors: simon.duckett@york.ac.uk and ian.fairlamb@york.ac.uk

The authors declare no competing financial interests.

ACKNOWLEDGMENT

We are grateful for financial support from the EPSRC (grant no. EP/G009546/1), Bruker BioSpin (CASE studentship KMA, and equipment). NWJS was funded by Bayer AG (PhD studentship). SBD and IJSF would like to thank the Wellcome Trust for funding (Reference Grants 092506 and 098335).

REFERENCES

1 (a) Nicolaou, K. C.; Bulger, P. G.; Sarlah, D. Palladium-Catalyzed Cross-Coupling Reactions in Total Synthesis. *Angew. Chem., Int. Ed.* **2005**, *44*, 4442–4489. (b) Torborg, C.; Beller, M. Recent Applications of Palladium-Catalyzed Coupling Reactions in the Pharmaceutical, Agrochemical, and Fine Chemical Industries. *Adv. Synth. Catal.* **2009**, *351*, 3027–3043. (c) Carole, W. A.; Colacot, T. J. Understanding Palladium Acetate from a User Perspective. *Chem.–Eur. J.* **2016**, *22*, 7686–7695. (d) Fairlamb, I. J. S. Redox-Active NO_x Ligands in Palladium-Mediated Processes. *Angew. Chem., Int. Ed.* **2015**, *54*, 10415–10427. (e) Devendar, P.; Qu, R.-Y.; Kang, W.-M.; He, B.; Yang, G.-F. Palladium-Catalyzed Cross-Coupling Reactions: A Powerful Tool for the Synthesis of Agrochemicals. *J. Agric. Food Chem.*

2018, *66*, 8914–8934. (f) Johansson Seechurn, C. C. C.; DeAngelis, A.; Colacot, T. J. Introduction to New Trends in Cross-Coupling. Colacot, T. J. (Ed) (2015), New trends in cross-coupling: theory and applications, Chapter 1, 1-19, Royal Society of Chemistry, Cambridge.

2 Ananikov, V. P.; Beletskaya, I. P. Toward the Ideal Catalyst: From Atomic Centers to a "Cocktail" of Catalysts. *Organometallics* **2012**, *31*, 1595–1604.

3 (a) Glasnov, T. N.; Findenig, S.; Kappe, C. O. Heterogeneous Versus Homogeneous Palladium Catalysts for Ligandless Mizoroki–Heck Reactions: A Comparison of Batch/Microwave and Continuous-Flow Processing. *Chem.-Eur. J.* **2009**, *15*, 1001–1010. (b) Lee, A. F.; Ellis, P. J.; Fairlamb, I. J. S.; Wilson, K. Surface Catalysed Suzuki–Miyaura Cross-Coupling by Pd Nanoparticles: An Operando XAS Study. *Dalton Trans.* **2010**, *39*, 10473–10482. (c) Astruc, D.; Lu, F.; Aranzaes, J. R. Nanoparticles as Recyclable Catalysts: The Frontier between Homogeneous and Heterogeneous Catalysis. *Angew. Chem. Int. Ed.* **2005**, *44*, 7852–7872.

4 Reay, A. J.; Fairlamb, I. J. S. Catalytic C–H bond Functionalisation Chemistry: the Case for Quasi-Heterogeneous Catalysis. *Chem. Commun.* **2015**, *51*, 16289–16307.

5 Leyva-Pérez, A.; Oliver-Meseguer, J. Rubio-Marqués, P.; Corma, A. Water-Stabilized Three-and Four-Atom Palladium Clusters as Highly Active Catalytic Species in Ligand-Free C–C Cross-Coupling Reactions. *Angew. Chem. Int. Ed.* **2013**, *52*, 11554 –11559.

6 Astruc, D. Palladium Nanoparticles as Efficient Green Homogeneous and Heterogeneous Carbon−Carbon Coupling Precatalysts: A Unifying View. *Inorg. Chem.* **2007**, *46*, 1884–1894.

7 (a) Fu, F.; Xiang, J.; Cheng, H.; Cheng, L.; Chong, H.; Wang, S.; Li, P.; Wei, S.; Zhu, M.; Li, Y. A Robust and Efficient Pd3 Cluster Catalyst for the Suzuki Reaction and Its Odd Mechanism. *ACS Catal.* **2017**, *7*, 1860–1867. For other studies showcasing the reactivity of related cyclic Pd_3 clusters, see: (b) Diehl, C. J.; Scattolin, T.; Englert, U.; Schoenebeck, F. C. C−I-Selective Cross-Coupling Enabled by a Cationic Palladium Trimer. *Angew. Chem., Int. Ed.* **2019**, *58*, 211-215. (c) Kalvet, I.; Magnin, G.; Schoenebeck, F. Rapid Room-Temperature, Chemoselective C_{sp2}-C_{sp2} Coupling of Poly(pseudo)halogenated Arenes Enabled by Palladium(I) Catalysis in Air. *Angew. Chem., Int. Ed.* **2017**, *56*, 1581–1585.

8 (a) Blanchard, S.; Fensterbank, L.; Gontard, G.; Lacte, E.; Maestri, G.; Malacria, M. Synthesis of Triangular Tripalladium Cations as Noble-Metal Analogues of the Cyclopropenyl Cation. *Angew. Chem., Int. Ed.* **2014**, *53*, 1987–1991. (b) Monfredini, A.; Santacroce, V.; Deyris, P.-A.; Maggi, R.; Bigi, F.; Maestri, G.; Malacria, M. Boosting Catalyst Activity in *Cis*-Selective Semi-Reduction of Internal Alkynes by Tailoring the Assembly of All-Metal Aromatic Tri-Palladium Complexes. *Dalton Trans.* **2016**, *45*, 15786–15790. (c) Monfredini, A.; Santacroce, V.; Marchio, L.; Maggi, R.; Bigi, F.; Maestri, G.; Malacria, M. Semi-Reduction of Internal Alkynes with Prototypical Subnanometric Metal Surfaces: Bridging Homogeneous and Heterogeneous Catalysis with Trinuclear All-Metal Aromatics. *ACS Sustainable Chem. Eng.* **2017**, *5*, 8205–8212.

9 (a) Scott, N. W. J.; Ford, M. J.; Schotes, C.; Parker, R. R.; Whitwood, A. C.; Fairlamb, I. J. S. The Ubiquitous Cross-Coupling Catalyst System '$Pd(OAc)_2$'/$2PPh_3$ Forms a Unique Dinuclear Pd^I Complex: An Important Entry Point into Catalytically Competent Cyclic Pd_3 Clusters. *Chem. Sci.* **2019**, *10*, 7898–7906. In hydrogenation/carbonylation chemistry it has been reported that cyclic hydrido Pd_3-type clusters are derived from a $Pd(OTf)_2$(P,P) complex (P,P = bidentate phosphine), see: (b) Baya, M.; Houghton, J.; Konya, D.; Champouret, Y.; Daran, J.-C.; Almeida Leñero, K. Q.; Schoon, L.; Mul, W. P.; van Oort, A. B.; Meijboom, N.; Drent, E.; Orpen, A. G.; Poli, R. Pd(I) Phosphine Carbonyl and Hydride Complexes Implicated in the Palladium-Catalyzed Oxo Process. *J. Am. Chem. Soc.* **2008**, *130*, 10612–10624.

10 Kannan, S.; James, A. J.; Sharp, P. R. $[Pd_3(PPh_3)_4]^{2+}$, a New Palladium Triphenylphosphine Complex. *J. Am. Chem. Soc.* **1998**, *120*, 215–216.

11 $[Pd(\mu\text{-}OH)(PPh_3)_2]_2[BF_4]_2$ complexes are not typically used as precatalysts. Other Pd^{II} precatalysts afford Pd^0 species, see: Serrano, J. L.; Garcia, L.; Perez, J.; Perez, E.; Garcia, J.; Sanchez, G.; Sehnal, P.; De Ornellas, S.; Williams, T. J.; Fairlamb, I. J. S. Synthesis and Characterization of Imine-Palladacycles Containing Imidate "Pseudohalide" Ligands: Efficient Suzuki-Miyaura Cross-Coupling Precatalysts and Their Activation To Give (PdLn)-L-0 Species (L = Phosphine). *Organometallics* **2011**, *30*, 5095-5109.

12 Lopez-Serrano, J.; Duckett, S. B.; Dunne, J. P.; Godard, C.; Whitwood, A. C. Palladium Catalysed Alkyne Hydrogenation and Oligomerisation: A Parahydrogen Based NMR Investigation. *Dalton Trans.* **2008**, 4270–4281.

13 Diver, C.; Lawrance, G. A. Trifluoromethanesulphonato-O Complexes of Platinum(II) and Palladium(II). *J. Chem. Soc. Dalton Trans.* **1988**, 931–934.

14 Omondi, B.; Shaw, M. L.; Holzapfel, C. W. Synthesis and crystal structures of new palladium catalysts for the hydromethoxycarbonylation of alkenes. *J. Organomet. Chem.* **2011**, *696*, 3091-3096.

15 (a) Amatore, C.; Bahsoun, A. A.; Jutand, A.; Meyer, G.; Ntepe, A. N.; Ricard, L. Mechanism of the Stille Reaction Catalyzed by Palladium Ligated to Arsine Ligand: PhPdI($AsPh_3$)(DMF) Is the Species Reacting with Vinylstannane in DMF. *J. Am. Chem. Soc.* **2003**, *125*, 4212–4222. (b) Ronson, T. O.; Carney, J. R.; Whitwood, A. C.; Taylor, R. J. K.; Fairlamb, I. J. S. AsCat and FurCat: New Pd Catalysts for Selective Room-Temperature Stille Cross-Couplings of Benzyl Chlorides with Organostannanes. *Chem. Commun.* **2015**, *51*, 3466–3469.

16 Szlyk, E.; Barwiolek, M. Studies of Thermal Decomposition of Palladium(II) Complexes with Olefin Ligands. *Thermochim. Acta* **2009**, *495*, 85–89.

17 Baumann, C. G.; De Ornellas, S.; Reeds, J. P.; Storr, T. E.; Williams, T. J.; Fairlamb, I. J. S. Formation and Propagation of Well-Defined Pd Nanoparticles (PdNPs) During C–H Bond Functionalization of Heteroarenes: Are Nanoparticles a Moribund Form of Pd or an Active Catalytic Species? *Tetrahedron* **2014**, *70*, 6174-6187.

18 Papp, S.; Dekany, I. Stabilization of Palladium Nanoparticles by Polymers and Layer Silicates. *Colloid Polym. Sci.* **2003**, *281*, 727–737.

19 Calvo, F.; Carre, A. Structural Transitions and Stabilization of Palladium Nanoparticles Upon Hydrogenation. *Nanotechnology* **2006**, *17*, 1292.

20 (a) Son, S. U.; Jang, Y.; Yoon, K. Y.; Kang, E.; Hyeon, T. Facile Synthesis of Various Phosphine-Stabilized Monodisperse Palladium Nanoparticles through the Understanding of Coordination Chemistry of the Nanoparticles. *Nano Lett.* **2004**, *4*, 1147–1151. (b) Hurst, E. C. PhD thesis, University of York (UK), 2009. (c) Hurst, E. C.; Wilson, K.; Fairlamb, I. J. S.; Chechik, V. N-Heterocyclic Carbene Coated Metal Nanoparticles. *New. J. Chem.* **2009**, 33, 1837-1840. (d) Cookson, J. The Preparation of Palladium Nanoparticles. *Platinum Metals Rev.* **2012**, *56*, 83–98.

21 Stakheev, A. Y.; Mashkovskii, I. S.; Baeva, G. N.; Telegina, N. S. Specific Features of the Catalytic Behavior of Supported Palladium Nanoparticles in Heterogeneous Catalytic Reactions. *Russ. J. Gen. Chem.* **2010**, *80*, 618–629.

22 McConnell, H. M.; McLean, A. D.; Reilly, C. A. Analysis of Spin-Spin Multiplets in Nuclear Magnetic Resonance Spectra. *J. Chem. Phys.* **1955**, *23*, 1152–1159.

23 Kullberg, M. L.; Lemke, F. R.; Powell, D. R.; Kubiak, C. P. Palladium-Palladium .Sigma.-Bonds Supported by Bis(dimethylphosphino)methane (dmpm). Synthetic, Structural, and Raman Studies of $Pd_2X_2(dmpm)_2$ (X = Cl, Br, OH). *Inorg. Chem.* **1985**, *24*, 3589–3593.

24 Murahashi, T.; Otani, T.; Okuno, T.; Kurosawa, H. Coupling of Alkynes on a Pd—Pd Bond to Generate an Electrophilic μ-Butenediylidene Moiety. *Angew. Chem. Int. Ed.* **2000**, *39*, 537–540.

25 (a) Lin, S.; Herbert, D. E.; Velian, A.; Day, M. W.; Agapie. T. Dipalladium(I) Terphenyl Diphosphine Complexes as Models for Two-Site Adsorption and Activation of Organic Molecules. *J. Am. Chem. Soc.* **2013**, *135*, 15830–15840. (b) Christmann, U.; Pantazis, D. A.; Benet-Buchholz, J.; McGrady, J. E.; Maseras, F.; Vilar, R. Synthesis and Computational Studies of Palladium(I) Dimers $Pd_2X_2(PtBu_2Ph)_2$ (X = Br, I): Phenyl versus Halide Bridging Modes. *Organometallics* **2006**, *25*, 5990–5995. (c) Takahashi, Y.; Tsutsumi, K.; Nakagai, Y.; Morimoto, T.; Kakiuchi, K.; Ogoshi, S.; Kurosawa, H. Mono- and Dipalladium Movement on the π-Conjugated Five-Carbon Chain. *Organometallics* **2008**, *27*, 276–280.

26 (a) Murahashi, T.; Kurosawa, H. Synthesis and Reactivity of Organopolypalladium Complexes. *J. Synth. Org. Chem. Jpn.* **2003**, *61*, 652–660. (b) Murahashi, T.; Ogoshi, S.; Kurosawa, H. New Direction in Organopalladium Chemistry: Structure and Reactivity of Unsaturated Hydrocarbon Ligands Bound to Multipalladium Units. *Chem. Rec.* **2003**, *3*, 101–111.

27 Montgomery, M.; O'Brien, H. M.; Méndez-Gálvez, C.; Bromfield, C. R.; Roberts, J. P. M.; Winnicka, A. M.; Horner, A.; Elorriaga, D.; Sparkes, H. A.; Bedford, R. B. The Surprisingly Facile Formation of Pd(I)–Phosphido Complexes from *Ortho*-biphenylphosphines and Palladium Acetate. *Dalton Trans.* **2019**, *48*, 3539–3542. (d) Wagschal, S.; Perego, L. A.; Simon, A.; Franco-Espejo, A.; Tocqueville, C.; Albaneze-Walker, J.; Jutand, A.; Grimaud, L. Formation of XPhos-Ligated Palladium(0) Complexes and Reactivity in Oxidative Additions. *Chem.–Eur. J.* **2019**, *25*, 6980–6987.

28 Godard, C.; Duckett, S. B.; Parsons, S.; Perutz, R. N. Dipyridylketone Binding and Subsequent C–C Bond Insertion Reactions at Cyclopentadienylrhodium. *Chem. Commun.* 2003, 2332–2333.

29 Yanai, T.; Tew, D. P.; Handy, N. C. A New Hybrid Exchange–Correlation Functional Using the Coulomb-Attenuating Method (CAM-B3LYP). *Chem. Phys. Lett.* **2004**, *393*, 51–57.

30 (a) Fairlamb, I. J. S.; Marrison, L. R.; Dickinson, J. M.; Lu, F.-J.; Schmidt, J. P. 2-Pyrones Possessing Antimicrobial and Cytotoxic Activities. *Bioorg. Med. Chem.* **2004**, *12*, 4285–4299. (b) Marrison, L. R.; Dickinson, J. M.; Fairlamb, I. J. S. Bioactive 4-Substituted-6-methyl-2-pyrones with Promising Cytotoxicity Against A2780 and K562 Cell Lines. *Bioorg. Med Chem. Lett.* **2002**, *12*, 3509–3513. (c) Collings, J. C.; Parsons, A. C.; Porres, L.; Beeby, A.; Batsanov, A. S.; Howard, J. A. K.; Lydon, D. P.; Low, P. J.; Fairlamb, I. J. S.; Marder, T. B. Optical Properties of Donor-Acceptor Phenylene-Ethynylene Systems Containing the 6-Methylpyran-2-one Group as an Acceptor. *Chem. Commun.* **2005**, 2666–2668. (d) Fairlamb, I. J. S.; Lu, F. J.; Schmidt, J. P. Palladium-Catalysed Alkynylations of 2-Pyrone (pyran-2-one) Halides. *Synthesis* **2003**, 2564–2670.

31 Miyaura, N.; Suzuki, A. Palladium-Catalyzed Cross-Coupling Reactions of Organoboron Compounds. *Chem. Rev.* **1995**, *95*, 2457–2483.

32 (a) Fairlamb, I. J. S.; Lee, A. F.; X. Ribas (Ed.), C–H and C–X Bond Functionalization. Transition Metal Mediation, RSC Catalysis (2013), pp. 72-107. (b) Reay, A. J.; Neumann, L. K.; Fairlamb, I. J. S. Catalyst Efficacy of Homogeneous and Heterogeneous Palladium Catalysts in the Direct Arylation of Common Heterocycles. *Synlett* **2016**, *27*, 1211–1216.

33 (a) de Vries, A. H. M.; Mulders, J.; Mommers, J. H. M.; Henderickx, H. J. W.; de Vries, J. G. Homeopathic Ligand-Free Palladium as a Catalyst in the Heck Reaction. A Comparison with a Palladacycle. *Org. Lett.* **2003**, *5*, 3285–3288. (b) Fairlamb, I. J. S.; Kapdi, A. R.; Lee, A. F.; Sanchez, G.; Lopez, G.; Serrano, J. L.; Garcia, L.; Perez, J.; Perez, E. Mono- and Binuclear Cyclometallated Palladium(II) Complexes Containing Bridging (N,O-) and Terminal (N-) Imidate Ligands: Air Stable, Thermally Robust and Recyclable Catalysts for Cross-Coupling Processes. *Dalton Trans.* **2004**, 3970–3981.

34 Scott, N. W. J.; Ford, M. J.; Eyles, A.; Simon, L.; Whitwood, A. C.; Tanner, T.; Willans, C. E.; Fairlamb, I. J. S. A Dichotomy in Cross-Coupling Site Selectivity in a Dihalogenated Heteroarene: Influence of Mononuclear Pd, Pd Clusters, and Pd Nanoparticles—the Case for Exploiting Pd Catalyst Speciation. *J. Am. Chem. Soc.* **2021**, *143*, 9682–9693.

35 (a) Sicre, C.; Alonso-Gómez, J. L.; Cid, M. M. Regioselectivity in Alkenyl(aryl)-heteroaryl Suzuki Cross-Coupling Reactions of 2,4-Dibromopyridine. A Synthetic and Mechanistic Study. *Tetrahedron* **2006**, *62*, 11063–11072. (b) Zhou, Q.; Zhang, B.; Su, L.; Jiang, T.; Chen, R.; Du, T.; Ye, Y.; Shen, J.; Dai, G.; Han, D.; Jiang, H. Palladium-Catalyzed Highly Regioselective 2-Arylation of 2,x-Dibromopyridines and its Application in the Efficient Synthesis of a 17β-HSD1 Inhibitor. *Tetrahedron* **2013**, *69*, 10996–11003.

Table of Contents

XPh_3 stabilized Pd_3 clusters detected en route to agglomerated Pd nanoparticles (PdNPs)